

NORTHWESTERN UNIVERSITY

System Design and Verification of the Precession Electron Diffraction Technique

A DISSERTATION

SUBMITTED TO THE GRADUATE SCHOOL
IN PARTIAL FULFILLMENT OF THE REQUIREMENTS

for the degree

DOCTOR OF PHILOSOPHY

Field of Materials Science and Engineering

By

Christopher Su-Yan Own

EVANSTON, ILLINOIS

First published on the WWW 01, August 2005

Build 05.12.07. PDF available for download at:
<http://www.numis.northwestern.edu/Research/Current/precession.shtml>

Appendices

APPENDIX A

Electronics Background

This section contains a review of some basic electronics that may be helpful for interpreting the circuit schematics in the PED implementations and understanding alignment procedures in later appendices. Discussion is limited based upon relevance to physical precession systems.

A.1. Limited-bandwidth systems

In feedback control theory, a *system* represents an entity to be controlled. It is treated as a black box with inputs and outputs, and the outputs exhibit a specific behavior for a given input. Such a system can be described by a transfer function (TF), a function of the frequency variable s , that describes its behavior. Here we will be concerned only with linear time invariant systems, which exhibit proportionality between cause and effect, and demonstrate additivity of effects (e.g., they obey the principle of superposition).

Beam deflector coils in the microscope are simple inductors that generate a response — a magnetic field, which deflects a beam of electrons — when current within the coil changes with time (e.g., response scales with dI/dt). They behave as low-pass filters when configured in series within a circuit, and can be modeled in feedback theory as a single-pole system P_{coil} in the series configuration, for example:

$$(A.1) \quad P_{coil} = \frac{1}{s + 5}.$$

A pole is a factor of s contained within the denominator of the TF.

This transfer function describes a coil with rather poor bandwidth and the output of the coil is much lower than the input, indicating losses within the coil. The attenuation requires an input that is 5 times larger in order to generate the desired response: if a response of 2 is desired, an input command of 10 must be provided. In this discussion, the units are simply “response units” as pertains to the desired output of system. It may be current, magnetic field, or deflection amplitude.

Bode diagrams describe the frequency-amplitude behavior of a system such as the one in equation A.1. It represents the amplitude response (frequency response) and the phase response of the system to a unity input over a range of frequencies. A sample Bode plot is shown in figure A.1(b) for the TF described in equation A.1 (its block diagram is given in figure A.1(a)). The figure shows that the system’s amplitude response is about 15 dB down at DC (0 Hz) and decays at 20 dB per decade. The system phase responds quite favorably with increasing frequency, never exceeding 90° phase delay behind the input.

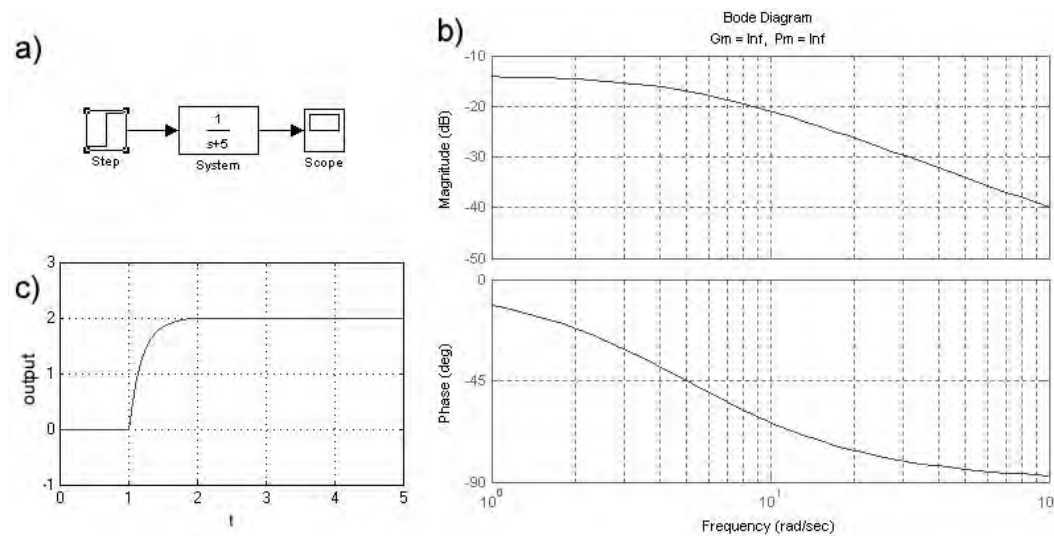


Figure A.1. (a) The block diagram for the system described by equation A.1. The Bode plot for this system is shown in (b), and the scope output showing the response to a step input of 10 units is displayed in (c).

The system is operated in single-ended mode, meaning that the system is given an input and is responsible for meeting the input with the appropriate output response; the system in this case does not monitor whether or not it has actually met the targeted output. The rise time at the output with response to a step input (infinitely steep) is relatively slow (about 1.7s, see figure A.1(c)), scaling with the time constant of the coil. Because the system is configured to be single-ended, it is susceptible to external factors such as oscillating magnetic fields that might alter the current in the coil at any given time.

This situation is not ideal for precise control of the system. Feedback is a solution: addition of feedback will give considerable improvements because it allows control of the current within the coil with the ability to correct for external disturbances, and it can be tailored to improve response. The system depicted in the block diagram in figure A.2(a) shows such a feedback network. In this case, some integrating electronics with effective transfer function $\frac{300}{s}$ are inserted in series, and a feedback loop with gain of 0.5 is installed around the two systems in series to provide the desired whole-system gain of 2. The effective transfer function of multiple systems in series is the product of their TF's, hence the TF of this feedback system can be calculated by taking the effective TF of the single-ended system divided by the sum, 1 + the TF around the feedback loop, giving:

$$(A.2) \quad G_{fb} = \frac{300}{s^2 + 5s + 150}.$$

The Bode plot in figure A.2(b) shows that the system response has been improved. A resonant peak occurs at about 5 rad/sec, and the step response (figure A.2(c)) shows a more rapid rise in output accompanied by some overshoot and then settling behavior to the steady state value. This system is optimized for rapid rise time, however such a coil control system would be deficient in many applications

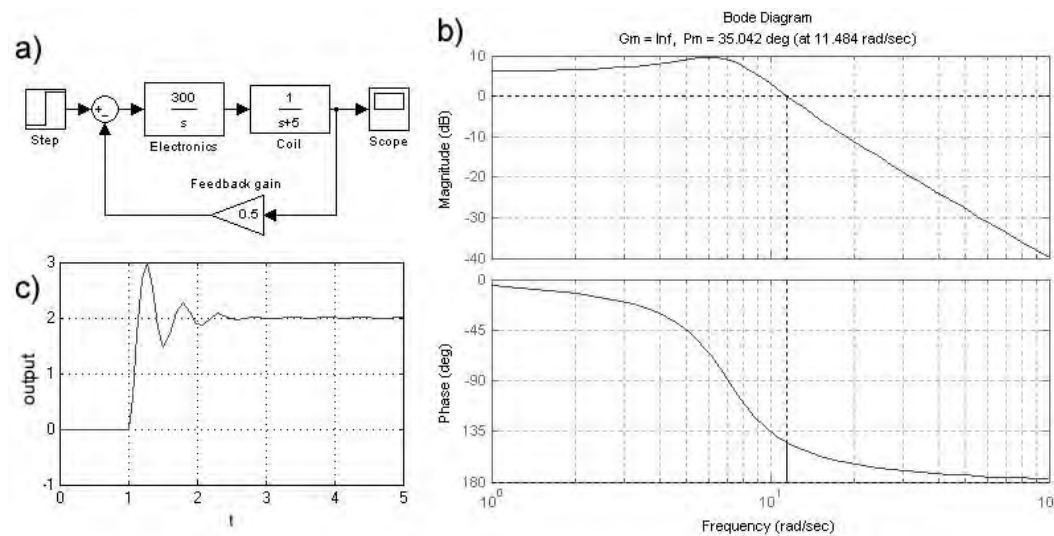


Figure A.2. (a) The block diagram for the system described by equation A.2. The Bode plot for this system is shown in (b), and the scope output showing the step response (1 unit) is displayed in (c).

because it is underdamped and does not settle rapidly. Further modification of the electronics transfer function with a different pole (e.g., changing the location of zeros in the denominator), or introducing higher order filtering (adding more poles to get higher powers of s in the denominator) can damp the overshoot and quell the ringing faster while not compromising rise time.

The bandlimiting occurs after the resonant peak with increasing frequency. The frequency response is 3 dB down by about 10 rad/sec and decreases in amplitude at a rate of 20 dB per decade. A second characteristic is that the phase of the oscillating signal varies between a few degrees to about -145° over its frequency bandwidth (180° phase lag corresponds to an unstable system). This is an important point because both BT and DS amplifiers will exhibit decreased output amplitude and increased phase lag as frequency increases. The result will be a change in the phase shift between the two coil sets when scanning frequency changes unless the coils and coil drivers are of the same type, the scanning frequency is low, or the system bandwidth is very high.

A.2. Amplifier design

The electronics used in the precession implementations of appendices B-D are based upon operational amplifiers (op-amps). Op-amps are complex feedback systems that are very versatile and easy to use for a variety of analog control and filtering applications. A short guide on how to implement basic op-amp circuits is given in this section. For advanced op-amp usage details, the reader is referred to an analog circuits textbook or IC application notes (Horowitz and Hill 1989; Franco 2002; Mancini 2002).

An ideal op-amp is shown in figure A.3. It exhibits very specific characteristics:

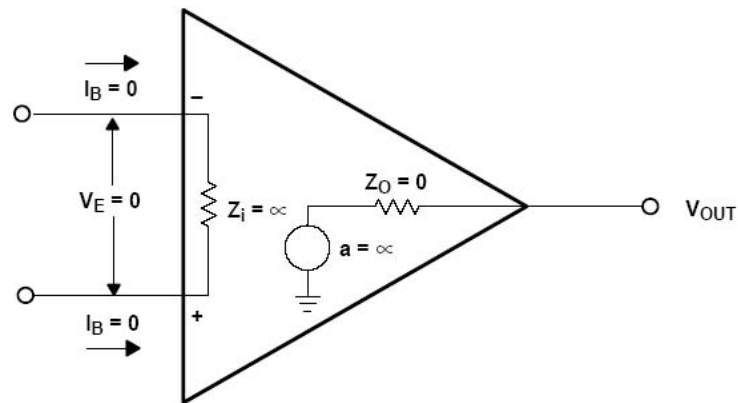


Figure A.3. The ideal op-amp (from Mancini (2002)).

- The two inputs (+ and -) have infinite input impedance: $z_{in} = \infty$. Thus, the inputs demand zero input current and do not load down the source.¹
- The op-amp has infinite gain on either input: $a = \infty$. When the op-amp is in single-ended configuration, a small voltage applied on either input will force the output to $\pm\infty$.
- The output impedance is zero: $z_{out} = 0$. The op-amp will therefore supply sufficient current to whatever load it is called upon to drive.
- The op-amp will do whatever it can to force the voltage difference between the inputs to zero: $V_e = 0$. This usually means that the output of the op-amp will change to meet this condition.

The application of feedback to the op-amp is what makes it a very powerful electronic component. A diagram of a common operational amplifier, the LM741 (in DIP8 package) is depicted in figure A.4. It possesses two signal inputs (inverting and non-inverting), one output, power supply inputs, and pins for offset nulling. Figures A.4(b)-(d) show the most basic configurations for amplification using this type of device. The non-inverting amplifier outputs a signal with the same polarity as the input waveform whereas the inverting amp naturally inverts polarity of the input. The gain of each configuration, shown to the right of each circuit in figure A.4, is set by a combination of the feedback resistor R_f and a second resistor R_i .

In circuit analysis terms, R_f and R_i represent a voltage divider (figure A.5(a)). The op-amp ensures that the two input terminals stay at the same voltage at equilibrium, thus the output terminal is forced to a voltage dependent upon the values of R_f and R_i . This can be determined by the voltage divider equation:

$$(A.3) \quad V_2 = \frac{R_i}{R_i + R_f} V_1$$

¹Impedance is the resistance to current flow dependent upon frequency in an AC system. Source impedance usually arises due to inductive effects.

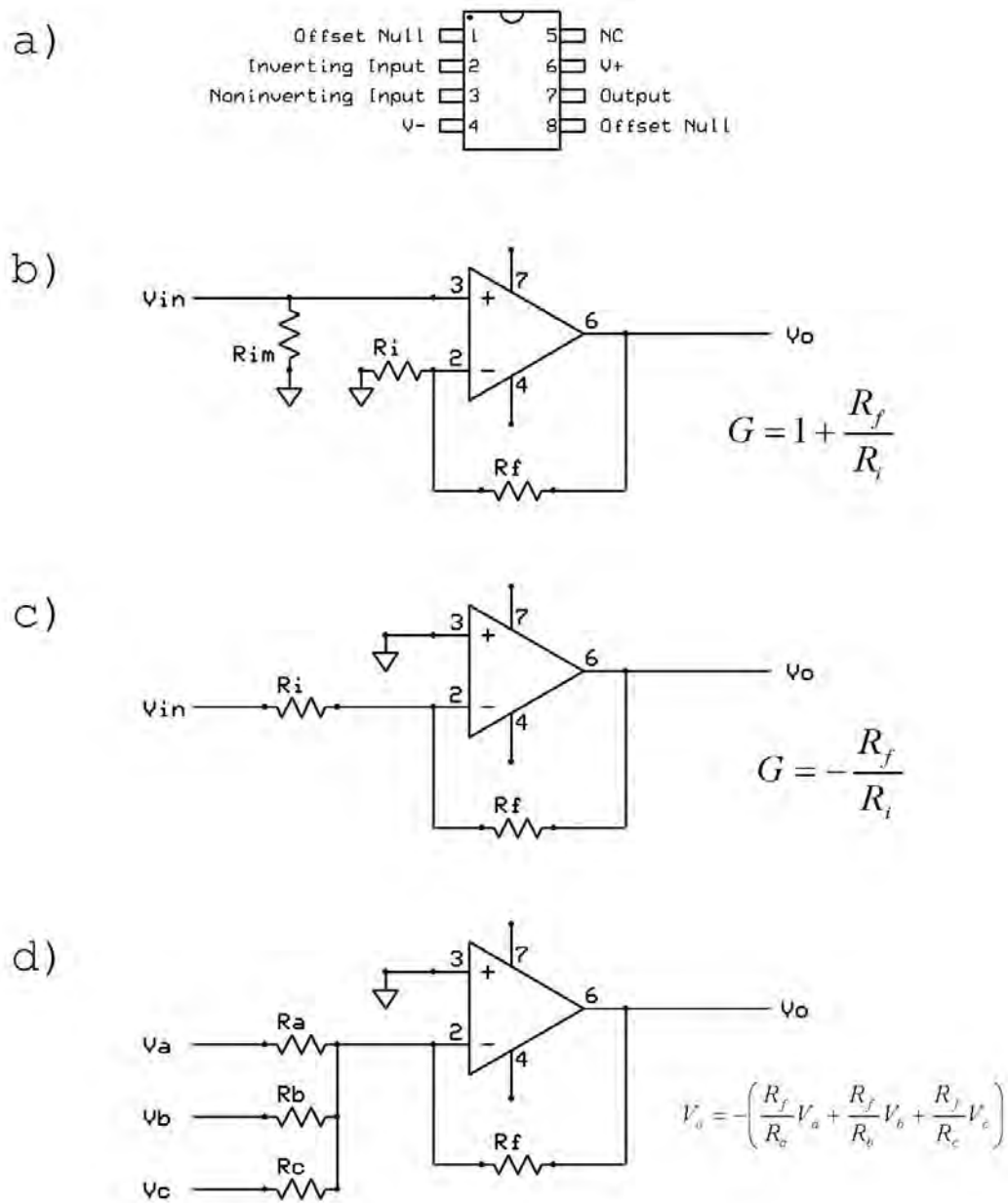


Figure A.4. (a) LM741 op-amp, DIP8 package. (b) Noninverting, (c) inverting, and (d) mixer (inverting) operational amplifier circuit configurations.

The output of the op-amp decreases the impedance at its connection to the voltage divider such that that terminal can drive (ideally) any downstream component. This is the reasoning behind a unity gain buffer stage, which does nothing other than convert impedances (and inverts the signal if configured to be inverting). In the mixer configuration, multiple input resistors are used which isolate the inputs from

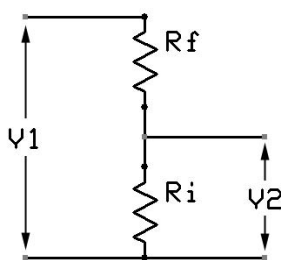


Figure A.5. Voltage divider.

each other. A relatively high value resistor (typically $> 1 \text{ k}\Omega$) is necessary to ensure that the inputs do not drive the others.

For precession, at least two inputs are necessary, one for steady-state control from the microscope console and the other for the oscillatory scan signal from the precession scan generator. In certain cases where the zero-point is significant (e.g., an “inputs-are-zeroed” indicator trigger), the amplifier may require offset trimming to remove voltage offset at the output. Some devices available on the market feature low intrinsic offset voltage to address this without user intervention.

Active filtering can be accomplished by adding capacitors or inductors to the feedback network. A simple low-pass filter was shown in 2.12(a), which results in a -3 dB point at a frequency of $\frac{1}{2\pi R_f C_f}$, where R_f and C_f are paralleled in the feedback loop. In feedback control theory, this represents an integrator, which produces a stronger negative feedback signal if the output does not respond as time passes. The capacitor time constant determines the bandwidth of the filter. Other configurations are available that provide high pass, band pass, or notch filtering behavior, the latter two generated by cascading different filter configurations in series. The reader is referred to reference texts for examples.

Real-world op-amps are naturally imperfect and are designed with compromises to meet specific application needs. Some basic constraints for selecting an amplifier device off the shelf for small signal buffering in precession are: high input impedance, moderate bandwidth, high power supply rejection ratio, and unity gain stability for the output buffer (second gain stage). FET-input (field-effect transistor) operational amplifiers that operate at unity gain in a moderate frequency range of DC to a few hundred kHz are quite suitable.

While operational amplifiers in general have excellent supply noise rejection, a well-designed power supply is nevertheless critical for performance. The supply should be able to deliver the current demanded by the amplifier rapidly (low supply impedance) and should have low noise to avoid poisoning the output signal with supply noise. Further, a split voltage supply is required for amplifying bipolar signals. The supply voltage rails should exceed the maximum signal amplitude by a fair margin to account for dropout voltage in the active devices, additionally it should be noted that many small-signal op-amps perform best when powered near their maximum rated supply voltage. Supplies of $\pm 15 \text{ V}$ are common in TEMs and it is often sufficient to use the on-board supply (commonly accessible from test points on the signal board) to power the precession electronics. Alternatively, an external supply can be

used so that the precession power supply is immune to fluctuations caused by circuits elsewhere in the microscope and vice versa.

Low supply impedance — already mentioned — is important for satisfying current demands. It is also crucial for amplifier stability and performance. The supply inductance can be decreased by decoupling the supply, synonymous with power supply bypassing. This is generally accomplished by providing a low impedance path to the amplifying device by placing extra capacitance near the device power supply leads. It is generally good practice to tier this: a high capacity electrolytic capacitor should be used, followed by a smaller low-ESR (equivalent series resistance) tantalum capacitor, and finally a low-loss, low-impedance film or ceramic capacitor of small capacity near the leads. The electrolytic capacitor is lossy and has high impedance compared to the others but it decreases power supply ripple by providing additional capacitance. Combination with smaller, faster, and low loss capacitors provides an extremely low impedance path to current reserves. A properly-bypassed op-amp will have better frequency response (closer to rated slew rate), and have less supply-related distortion at its output.

A.3. Simple Linear Power Supply Design

The type of power supply used in the later precession implementations is a simple regulated linear supply using off-the-shelf active regulator components. Linear power supplies are less efficient than switching power supplies commonly found in electronics, however, they exhibit much lower noise so are preferred in this application. A conventional linear supply comprises three main stages, a transformer to convert the AC mains voltage into an AC voltage with amplitude suitable for the electronics being supplied, a rectification stage to rectify the waveform polarity, and filtering (including regulation) to store the charge and/or reduce the ripple to form a stable supply voltage. Figure A.6(a) shows a simple LC supply that incorporates a full-wave bridge rectifier.

In this supply, a transformer with internal resistance of $31\ \Omega$ supplies a 48 VRMS AC waveform to the bridge rectifier. Specifically, the primary winding of the transformer accepts 120VAC and the secondary winding outputs 48VAC, meaning the turns ratio between primary and secondary is about 2.5. The bridge is designed such that the top legs only conduct positive current and the bottom legs conduct only negative current, rectifying the voltage. The rectifier bridge is a full wave rectifier, so charge is being conducted during all parts of the AC waveform. The bottom legs may be fixed to a reference such as ground, forcing the top of the bridge to be positive with respect to that reference. An LC filter follows. The 1 H inductor acts as a current choke, limiting large current flow except when demand is very high. Referring to figure A.6(b), the steady state behavior of the inductor is a mild oscillation of about 25 mA peak-to-peak that charges the capacitor C1 between AC waveform rectification cycles. The time constant of the $220\ \mu\text{F}$ capacitor is on the order of 700 s, therefore the capacitor does not discharge much into the $5\ \text{k}\Omega$ load R1 during each AC cycle. The inductor, L1, whose time constant is much lower, is able to effectively replenish the charge being drawn from C1 by the load.

The start-up behavior is the most stressful part of operation and components must be chosen to endure the turn-on conditions. During a period of about 50 ms, the capacitor acts as a short circuit, demanding as much instantaneous charge as can be supplied through the inductor. The current through the inductor peaks at about 410 mA and then declines to steady state behavior as the capacitor nears

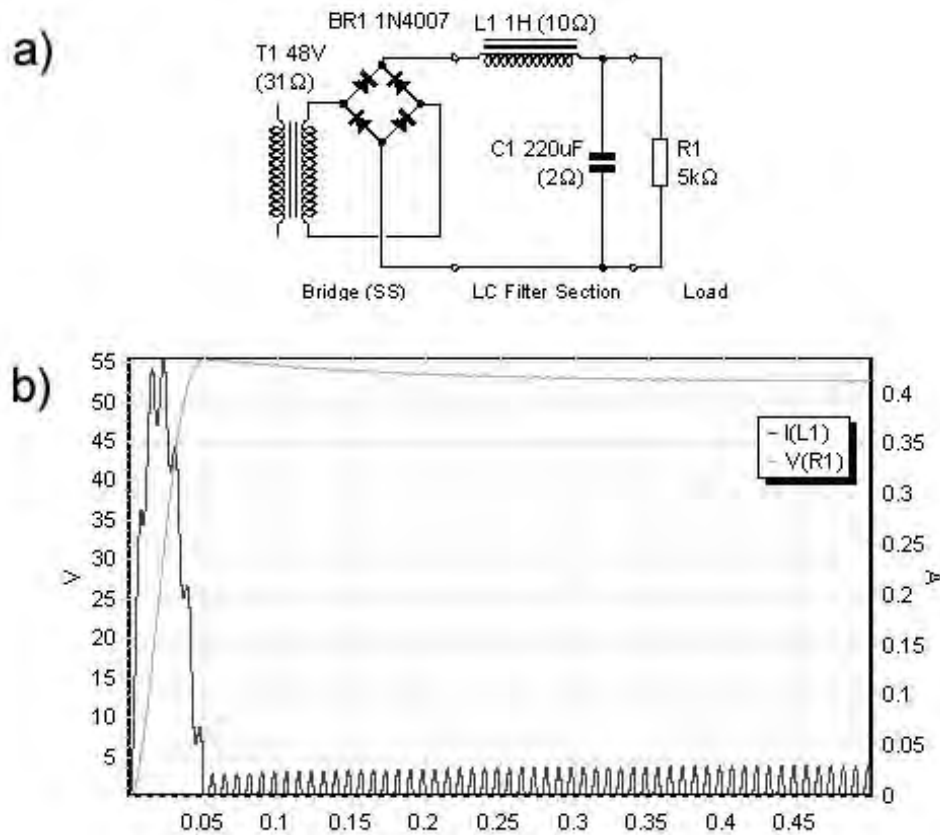


Figure A.6. (a) Full-wave 48V LC unregulated supply. (b) The current and through the inductor L1 and the voltage supplied to the load $V(R1)$. The turn-on behavior results in a spike in current and a slow build-up of supply voltage with stabilization by about 300ms.

full charge. C1 experiences a slight overshoot before settling to the steady state loaded voltage of ≈ 52 V. The rectifier must have sufficient headroom (typically a factor of two or three) to handle the large instantaneous current demanded by the supply at turn-on. In this case, rectifier diodes rated at 1-1.5 A would be desired.

Split supplies simply fix a reference voltage in between the two voltage rails. Since the secondary windings and rectifier are floating (they do not reside at an absolute voltage), it will graciously supply the full voltage across the secondaries and the downstream electronics divide this as necessary to provide positive and negative voltages.

If the supply is more heavily loaded, this voltage may sag. Regulation is the solution to this problem. The raw DC voltage provided by the supply in figure A.6 can be fed into a regulation stage, a feedback system itself, which monitors the output voltage and keeps it at the same value regardless of load (lowers

supply impedance). Regulators are often made from discrete components, however monolithic three-terminal fixed-voltage regulators are quite straightforward to use — they are simply placed in series with the supply leads and a reference pin is tied to an appropriate voltage reference. Usage details can easily be found in datasheets for off-the-shelf components.

APPENDIX B

Implementation 1

B.1. Hitachi H-9000 retrofit

The Hitachi UHV H-9000 is a 300 kV instrument designed for high resolution imaging and diffraction. The instrument incorporates a special SA imaging mode for selected area diffraction experiments intended to minimize SA errors. Because the system has a small objective polepiece gap, the stage allows only about $\pm 10^\circ$ tilt and the UHV side insertion system has been designed without z -height adjustment for mechanical simplicity.

A stacked pair of coils (a dipole and quadrupole deflector) located several centimeters above the objective polepiece gap provides BT deflections. DS deflections are provided by a dipole deflector nested inside the projector lens. Upper column electronics can be found on the board BD STB under the left console, and image shift is controlled from a small potentiometer box that controls an amplifier board mounted the left console side, called Image S. The relevant section of the BD STB schematic is shown in figure B.1 Each beam tilt axis is set using a digital encoder that controls a DAC (not shown) followed by a small unity gain buffer. This signal is in the range of ± 5 V and supplies the BTX and BTY inputs on connector CN3503. Section I in the figure is part of an analog hollow cone driver called STIG MON for monitoring astigmatism in the objective lens (not active during normal operation). Following is the tilt amplifier (II) comprising an op-amp in summing mode driving a FET-output voltage-to-current amplifier. There is some biasing circuitry in this stage that ensures sufficient bandwidth for the tilt wobbler adjustment, favorable for precession because it offers operation up to about 1 KHz. Section III is a voltage divider and switching array used to split the current between the three coil windings for each tilt axis. Four user-accessible potentiometers in this stage control the division of current to each winding: these are the X_{main} , X_{vert} , Y_{main} , and Y_{vert} controls used during shift-tilt purity alignment.

The custom modules described in section 2.5 (figure 2.12) were retrofitted at points a and b in series with the input CN3503. The modules were built around an LM324 integrated circuit in DIP14 package (a quad 741 IC with class AB biasing). The BT mixer module was mounted onto a short length of 34-conductor ribbon cable that also serves as a quick-release pass-through extender for connector CN3503. Conductors 3 and 5 on the cable, corresponding to pins 2 and 3 of CN3503, were used to insert X and Y signals, respectively, and conductor 1 was used for the ground reference. Power was supplied to the add-on boards via the ± 15 V supply pins on the BD STB and Image S. boards.

The image shift circuit is intended for steady state operation and is correspondingly quite different from BD STB (figure B.2). The signal originates from a 10 V precision reference (I.), converted into ± 4 V reference legs (II.) by an op-amp stage. These are divided into control voltages by linear potentiometers (III.) followed by a differential op-amp buffer stage (IV.) that feeds the coil amplifier

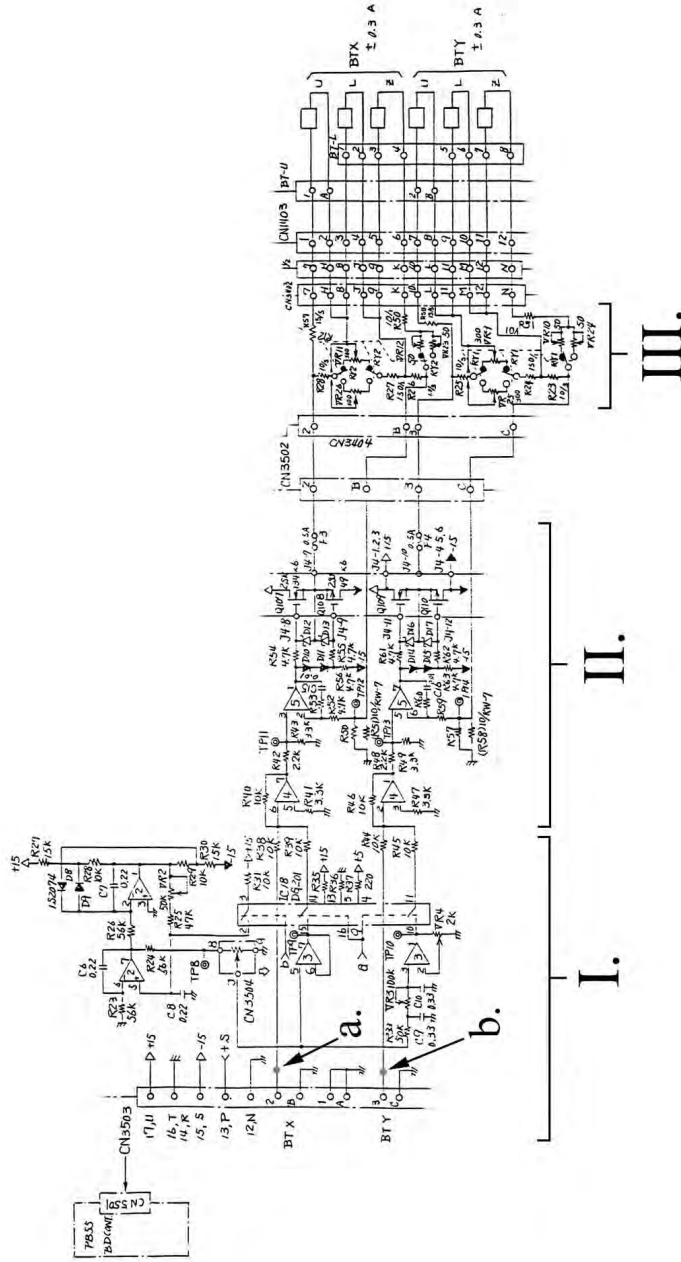


Figure B.1. BD STB circuit, Hitachi H-9000. Courtesy of Hitachi High Technologies.

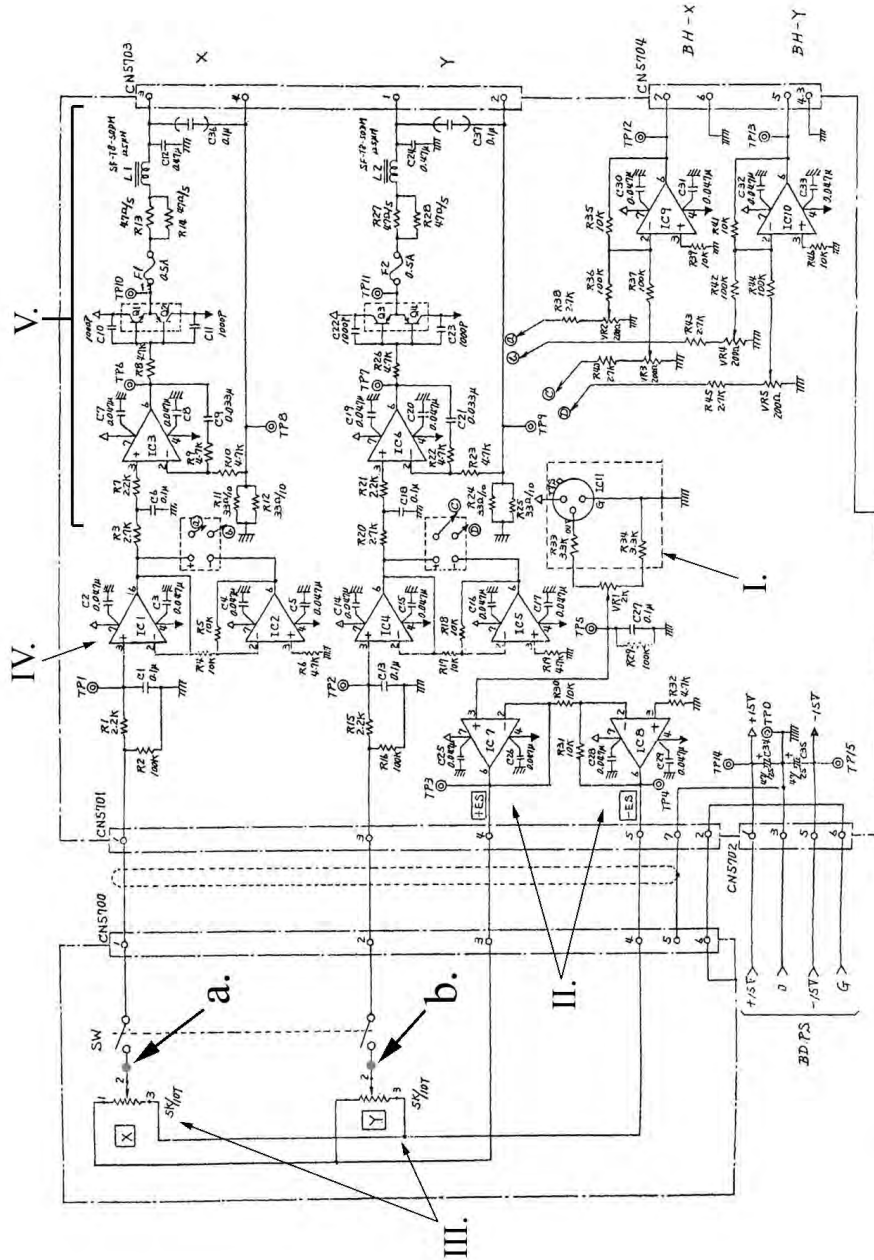


Figure B.2. Image S. circuit, Hitachi H-9000. Courtesy of Hitachi High Technologies.

(V.). The inverted leg of the differential buffer (not connected in this instrument) provides an optional compensation signal for an extra dipole deflector (BH-X,Y) earlier along the optic path. The DS current amplifier terminates in a bipolar push-pull output stage that delivers larger currents than the BT (around several hundred milliamps) to achieve appreciable deflections of the image on the viewing screen. The circuit is precise and has low noise for image stability.

While excellent for DC signals, the stock image shift circuit was found to be unsuitable for precession due to the class B problem (see section 2.5.1 for details). Push-pull amplification stages, if not properly biased, can cause distortion at the zero-crossing point of rapidly varying signals because each device in the complementary pair has a finite switching time. A possible solution was to bias the output stage into class A to remove the distortion, however working around the design proved difficult and the final solution took the form of a completely redesigned board based on power op-amps shown in figure B.3. This preserves the service warranty for the instrument and provides extra performance headroom. The Image S. circuit is broken at R3/R20 and the output of the preceding driver stage is routed directly to the custom DS amplifier board, bypassing the stock amplifier. The replacement amplifier consists of an OPA544T power operational amplifier in a current-sense feedback loop similar to that used in the stock circuit. Power and ground are supplied from Image S. and additional supply filtering is employed. The replacement unit extends usable bandwidth beyond 2KHz.

Figure B.4 contains photographs of the completed UHV H-9000 precession implementation demonstrating the installation locations.

B.2. Performance and limitations

The precession mode is typically operated at about 60 Hz to ensure ample intensity averaging for short exposures. During operation, an artifact often appears in the scan due to power supply ripple identified by a “snail” (a small kink in the circle pattern) that travels slowly around the BT circle. Its speed depends on the relation between the scan and mains frequencies. The artifact can be removed by precisely matching the scan rate with the oscillation frequency of the mains. This can vary throughout the day, depending on the mood at the power company. On-site, the mains frequency typically varies between about 59.25 Hz to 60.25 Hz and can change during a microscopy session.

The H-9000-based precession instrument is limited by its lack of eucentric height adjustment and small tilt range ($\pm 10^\circ$). Depending upon insertion conditions, the specimen height may deviate from optimum crossover by over 100 μm , limiting the spatial resolution of the precession probe. The shift-tilt purity correction range is insufficient to localize the probe. To circumvent this problem, precession is typically operated with selected-area mode using parallel illumination: the SA aperture limits probe wandering by ensuring even illumination of the specimen. However, the smallest probe size becomes limited by aperture size, and SA errors give rise to excess delocalization of illumination that cannot be avoided because optimum lens excitation and specimen height are unavailable (Hirsch et al. 1965).

Poor probe localization is the ultimate limitation of this system, making nanocrystal precession diffraction studies difficult. The instrument nevertheless acquired patterns from large regions and isolated small particles rather well, giving good averaged patterns from sample regions about 200 nm in

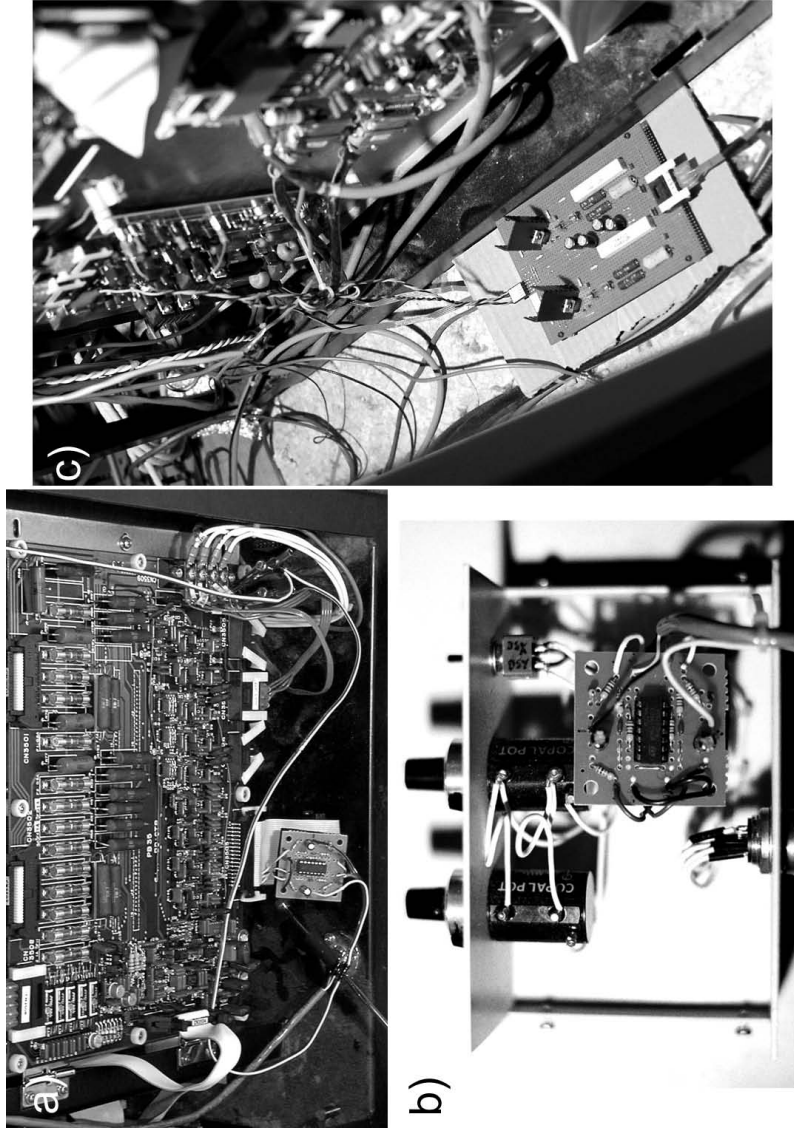


Figure B.4. The hardware for the first-generation precession instrument installed on the Hitachi UHV H-9000. (a)-(b) BT and DS signal insertion modules. (c) Replacement DS coil driver of figure B.3.

diameter. Measurable patterns have been acquired from $\text{Mg}_3\text{V}_2\text{O}_8$ and $\text{La}_4\text{Cu}_3\text{MoO}_{12}$ with this machine (Own et al. 2004). For the $\text{La}_4\text{Cu}_3\text{MoO}_{12}$ experiments, the cone angle of 25 mrad was large for this instrument and the spots became ill-defined and difficult to measure. Rather than employing the more accurate method of cross-correlation using average unitary spot motif (requiring similarly-shaped spots), the intensities from this pattern were integrated after background subtraction from small masked regions around each spot. This quantitation method is described in appendix F.

APPENDIX C

Implementation 2

C.1. JEOL 2000FX Retrofit

A second-generation precession instrument was constructed based on the JEOL 2000FX microscope chassis located at UOP, LLC in Des Plaines, Illinois. The 2000FX is an analytical instrument well suited for precession since the polepiece supports high tilts by virtue of a well-developed convergent beam mode. The instrument included a $\pm 45^\circ$ side-entry double-tilt holder and a model US1000 2K \times 2K CCD camera from Gatan, Inc. This implementation drew upon the knowledge gained from the previous precession implementation and integrated some refinements that improved performance dramatically:

- (1) Specimen holder z -height adjustment;
- (2) The polepiece supports large tilts;
- (3) A large CCD streamlines dataset acquisition;
- (4) Beam blanking above specimen decreases radiation damage;
- (5) Miniaturized plug-in modules using surface mount devices;
- (6) Independent power supply (external);
- (7) Improved grounding scheme;
- (8) Updated software.

Photographs of this implementation are shown in figure C.1.

The 2000FX deflector electronics are located on a single board DEF UNIT, which controls all deflector coils in the column (accessible below the right-hand console behind an acrylic cover). The current values for each coil set, controlled by a pair of digital encoders, is stored in memory and held constant by the microscope computer, changing only when console control is passed to that coil set. The power amplifier design is common to most of the deflectors in the instrument and is simply replicated in each coil driver circuit down the column. The 2000FX has provisions for a hollow-cone illumination option, thus its deflectors can process fast scan signals without modification.

Block diagrams for the BT and DS amplifiers are displayed in figure C.2. Coils COND1,2X,Y provide BT deflections, and PROJX,Y denote the DS deflectors. For precession, the location at which the digital stage feeds the analog stage is an ideal location to insert the scan signal. The mixer modules can simply be inserted in series before resistors R63, R70, R103, and R106, corresponding to BTX, BTY, DSX, and DSY.

The plug-in modules (figure C.3(a)) were based on Burr-Brown OPA2604 dual operational amplifiers in SOIC8 package — low noise amplifiers designed for audio. Most of the electronics were

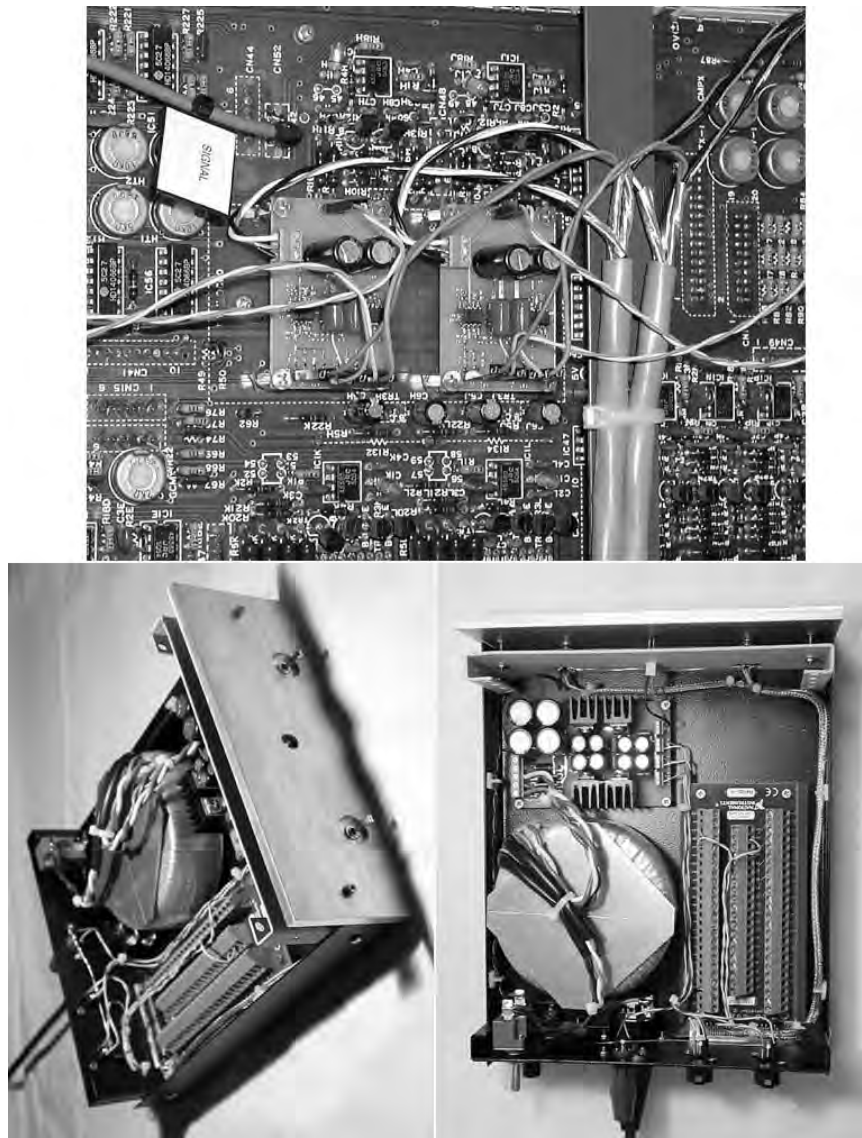


Figure C.1. The hardware for the second-generation precession instrument. Left: outboard power supply and signal distribution box. Right: Plug-in signal insertion modules.

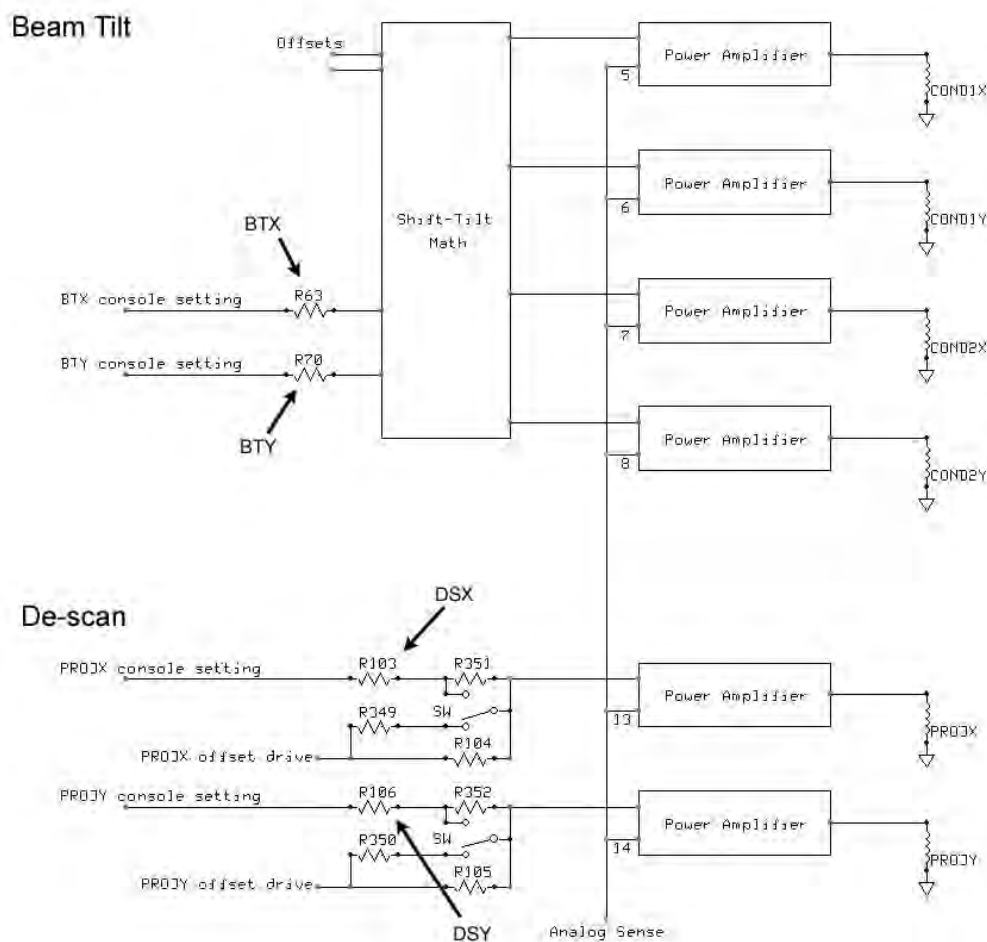


Figure C.2. DEF UNIT block diagram for the JEOL 2000FX. BTX, BTY, DSX, and DSY indicate the locations where the plug-in module should be inserted.

migrated to surface mount technology, easing installation by virtue of miniaturization. A simple dedicated linear regulated supply, comprising capacitive decoupling between two regulation stages, was built for the plug-in modules (figure C.3(b)). JEOL specifies < 10 mV ripple for the DEF UNIT, which the custom supply meets. The power supply and a National Instruments signal distribution board were incorporated into a project box that included BT and DS on/off toggle switches on the front panel for manual control independent of software. The PC DAC board interfaces with the project box via a 68-pin high-density cable, upper and lower coil outputs on the rear panel incorporate power leads and signal lines (isolated from each other via foil shields) into a single cable bundle for each module, and an additional terminal for the microscope ground is also provided. The ground connection from the microscope is shorted to the PC ground and can be broken with a toggle switch when precession is not in use.

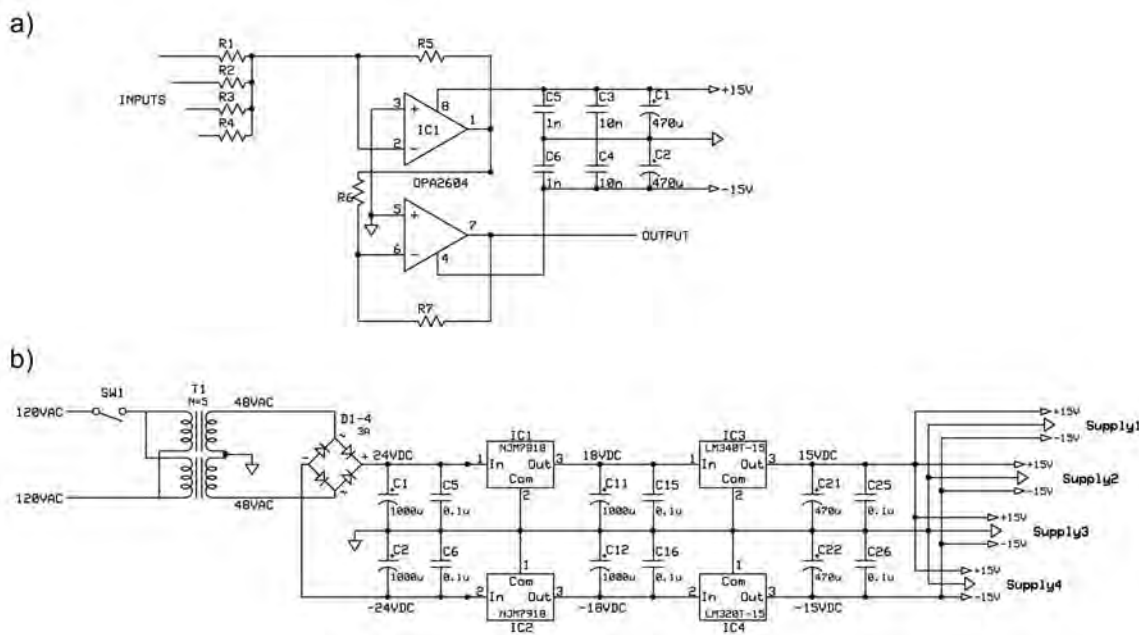


Figure C.3. Schematics for the second generation precession system. The plug-in modules are shown in (a) and the outboard power supply, capable of powering up to four modules, is shown in (b).

C.2. Performance and limitations

The instrument is operated in Koehler mode (see section 2.3) with smallest condenser aperture and spot size for small probe, coherence, and low dose to protect the CCD. BT on the 2000FX can be operated in either a bright mode or dark mode. In the latter, the control input is multiplied by a factor of 10 to increase the tilt control sensitivity. It is advantageous to operate in the bright mode to make best use of the scan generator's dynamic range. A scan amplitude of 3.5 V yields about 40 mrad in this mode.

Careful alignment of the precession device yields very high quality patterns (the procedure is given in appendix E). Figure C.4(a) is a montage of probe images at several points along the precession route for a near-aligned condition. The probe has been spread to about 50nm to clearly show the crystal edge. Each tile in the montage contains a different image of the specimen representing a specific tilt condition, and for each scan step the beam becomes slightly displaced from the centered beam in the image plane (not apparent in the figure). This probe wandering causes delocalization when the beam is precessed at full speed. The center image is the composite of the full precession; the specimen image becomes blurred and the probe becomes delocalized if alignment is poor. Moving the specimen closer to eucentric height and optimizing the lens settings and aberration compensations improves both localization of the probe and sharpness of the specimen features (figureC.4(b)).

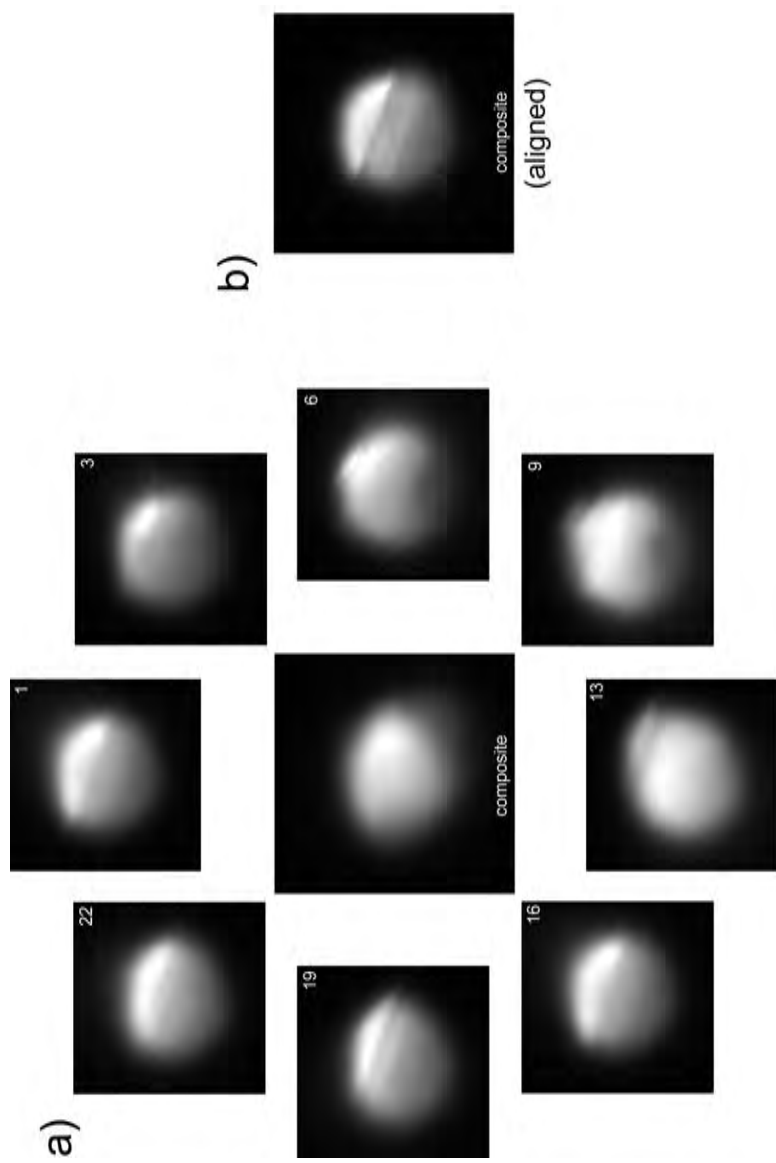


Figure C.4. (a) Montage of probe images during a precession revolution (close to aligned). 24 frames denote a full revolution; 8 of 24 are shown here. The center image shows the composite of all tilts. Both probe and specimen image wander for in the unaligned condition, contributing to a blurry composite image. The right image (b) shows a well-defined specimen image and excellent alignment of the cone pivot point after alignment. Probe size is ≈ 50 nm.

The 2000FX implementation can generate usable patterns using cone semi-angles of up to about 50 mRad. Appreciable projector distortions result beyond this point, as seen in figure 2.14(a), but patterns may still be measurable if integration methods less sophisticated than auto-correlation are used. The highest quality patterns are obtainable using cone semiangle between 0 and 40 mrad (see for example figure 2.14(b)); probe localization is excellent up to about 35 mrad, yielding approximate probe size of 25 nm for a very well-aligned experiment. A larger 50 nm probe is readily achievable with about 15 minutes of alignment time. The 2000FX instrument has been used to obtain high-quality precession patterns for particle regions as small as 30 nm.

APPENDIX D

Implementation 3

D.1. JEOL 2100F

At the time of this writing, a new precession implementation has been designed for installation on a JEOL 2100 analytical microscope. The design principle is similar to the previous PED systems described in these appendices. The new system is designed for more portability and should be more easily retrofittable to most microscopes. The power supply in the signal distribution box has been improved and the unit uses differential drivers to send the signals to the microscope. Differential receivers at the microscope receive the signals and apply them to the appropriate summing junctions in the deflector electronics.

The receivers can be powered by the microscope circuit or by the onboard supply. Ground is not shared between the control box and the microscope, thus avoiding common mode noise and preventing noise from filtering into the microscope circuits from the control computer. Some additional functionality has been designed in, such as receiver circuit disable (allowing precession to be switched out of the microscope system completely by the control computer) and some health status monitoring. Up to 8 channels are available in the case that double-deflectors are used for both scan and descan. The signals are provided by a NI PCI-6733 16-bit DAQ board.

Schematics for a version of the new system that use single-ended signaling are given on the following pages.

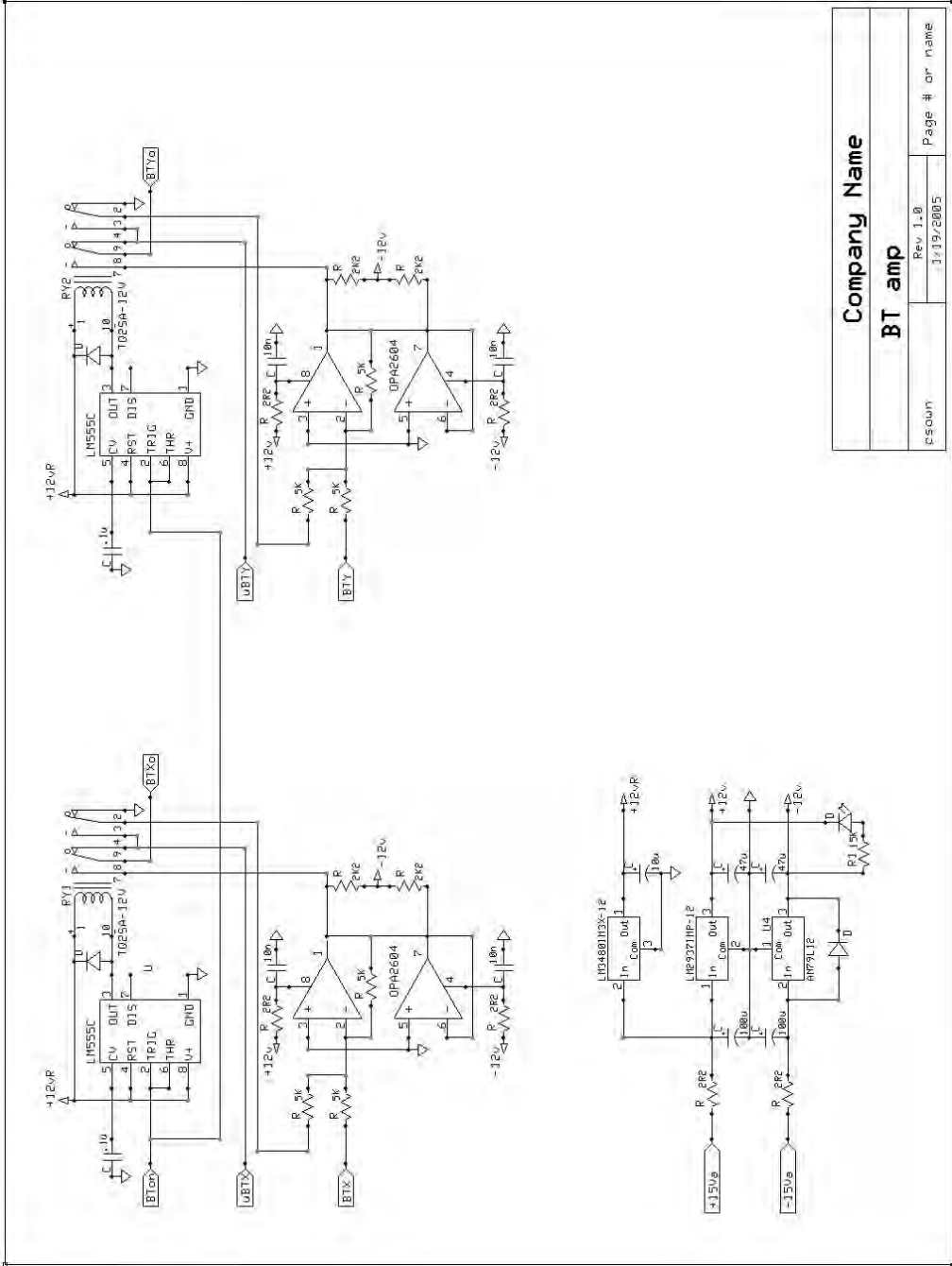


Figure D.2. BT signal board schematics for the new PED system.

APPENDIX E

Alignment Procedure

Alignment of the precession system is similar to conventional column alignment, e.g., from the gun toward the detector. With the column previously aligned for imaging, the precession alignment described here is straightforward and can typically be completed within about 15 minutes.

The following conditions are required for a high-quality precession experiment:

- (1) Specimen on-zone to within ± 1 mrad. Precession patterns are quite tolerant of a slightly off-zone condition, but a better on-zone condition will yield better accuracy in the intensity integration;
- (2) Specimen located close to or at eucentric height in the z -direction;
- (3) Beam well-aligned with the optic axis (HV centering);
- (4) Diffraction spot carefully focused and intermediate lens stigmatism corrected;
- (5) De-scan coils roughly zeroed to minimize deflector nonlinearity and avoid parallax distortions;
- (6) If a CCD camera is used, spot size and convergence set so as to not over-expose the camera.

Highest tilt is achievable when the objective lens system is excited to its optimal current setting: this is the point where lens aberrations are lowest and smallest probe size is possible. Optimal objective excitation is factory-specified and can be obtained from the microscope manufacturer. Objective excitation is the most important parameter in the precession experiment, and the alignment of the system derives from this starting point.

The procedure for alignment is detailed pictorially in the flow diagram in figure E.1. The objective should be optimally excited and the region of interest (ROI) located at optimum focus. After conventional alignment of the imaging system, precession alignment begins by exciting the scan in the upper tilt coils (BT) to the desired cone angle in diffraction mode. One can determine cone angle by referencing the scan against diffraction spots or a calibration pattern. With scan on, switching to image mode will yield a circle that shows the intersection of the hollow cone with the specimen. The circle may be distorted due to objective aberrations. If the scan rate is lowered to below 1 Hz, one can easily see the beam tracing a path in real space through the aberrations in the lens field.

Shift-tilt purity correction (sometimes also called tilt wobbler alignment) should be adjusted next to obtain the smallest and least distorted ring pattern possible. This adjustment aligns the stacked BT deflector coils, compensating for rotations and minor dipole non-uniformities. Since the beam is swept around a perimeter inside the tilt coil, the adjustment may not result in the same shift-tilt purity settings as the conventional two-axis tilt purity adjustment, which sweeps only along the two major axes.

Continuing in real space, beam convergence should be re-adjusted if necessary to obtain minimum probe size. This will generate a fine ring pattern (though possibly distorted). If the tilt purity correction

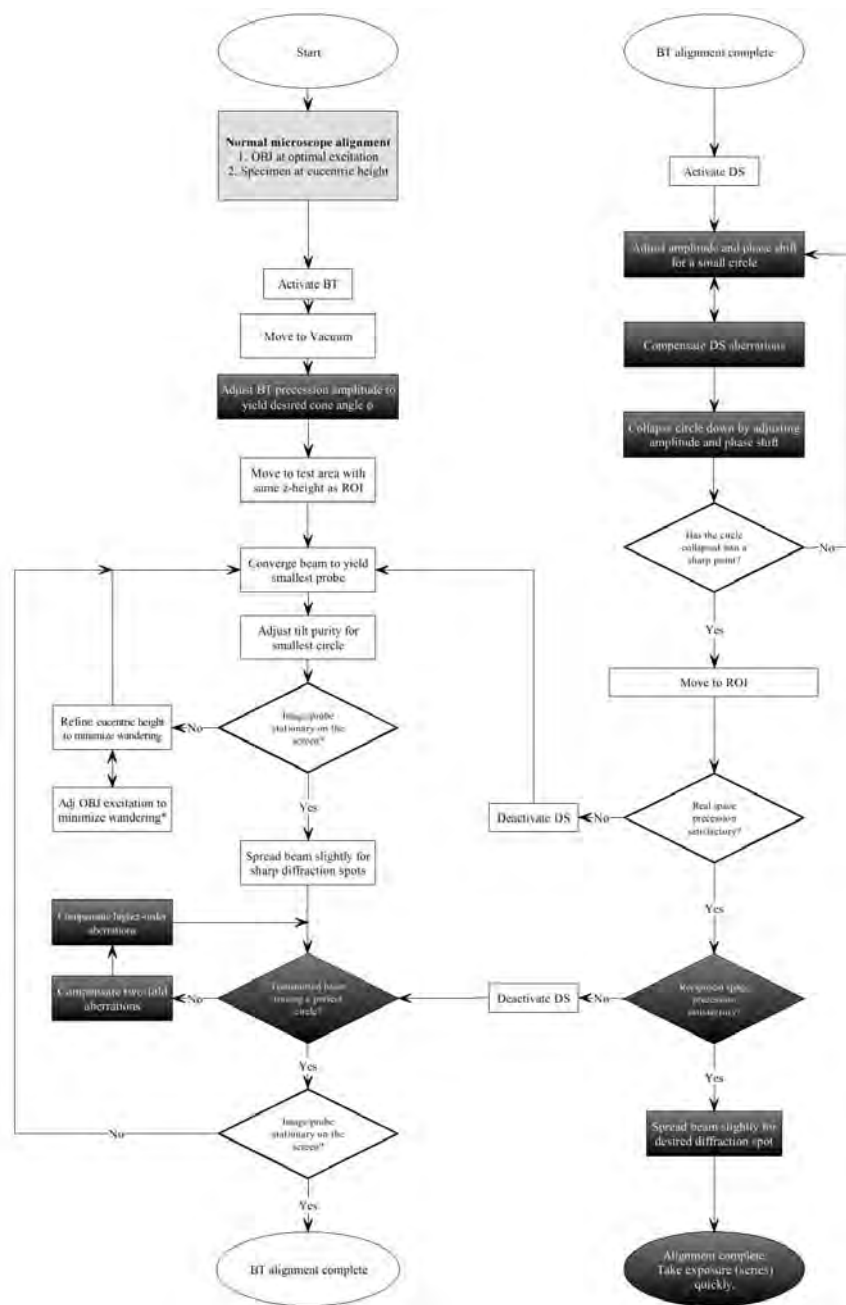


Figure E.1. Alignment procedure for the PED systems described in appendices B-C.

forms a fine spot and the specimen image moves minimally with BT scan active, the real space tilt alignment is complete. If not, specimen height must be adjusted to better intersect the convergence point of the cone and subsequent refinement must be carried out. The three variables — objective

excitation, sample height, and tilt purity — can be iteratively refined in this way until a reasonably stationary hollow cone probe and sample image are achieved in real space.

The next step is to refine the reciprocal space behavior of the BT precession. This is demonstrated in figure E.2. It is usually convenient to do this alignment off the specimen in vacuum to make use of a sharp and bright transmitted beam. In diffraction mode, the scan parameters on the precession control panel can be used to compensate for the aberrations and make the ring round. If digital capture is available, one can use a circle overlay as a reference for applying the compensations until the pattern is incident to or concentric with the reference circle (figure E.2(a)). If the real space alignments were done well, these compensations should have little or no effect on the real space behavior of the beam. Otherwise, refinement of real space alignment may be necessary after BT alignment in reciprocal space. If the scanned circle in diffraction space is concentric and the real space image and probe are stationary, BT alignment is complete.

Once beam tilt alignment is complete, de-scan can be activated (figure E.2(b)). The procedure for DS alignment is easier and less sensitive than the BT. The software implementation has real-time updates, so one can simply “wobble” the slider bars for DS amplitude and phase shift to perturb the de-scanned pattern, revealing the direction in which the alignment should progress in order to collapse the BT circle down to a sharp spot. Elliptical compensations for two-fold distortions can be applied concurrently to form a sharp point. Moving the specimen into the path of the beam allows the user to check the quality of the alignment for higher angle reflections.

Once the alignment of the transmitted beam is complete and a high quality zone axis pattern is obtainable, it is advantageous to double-check real-space alignment before switching to precession mode

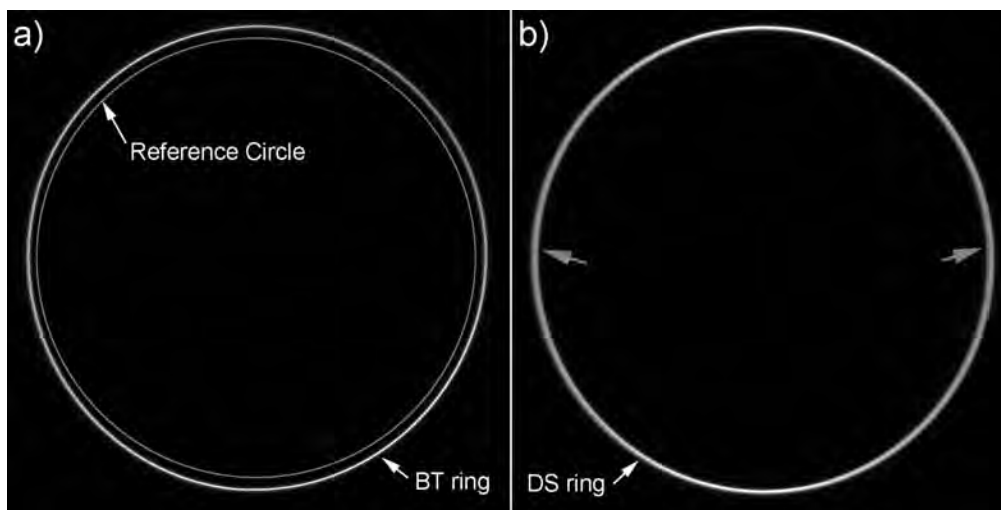


Figure E.2. Reciprocal space alignment on the JEOL 3000F systems described in appendix C. (a) shows the BT ring alignment and (b) shows the complementary descanned alignment. The x and y descanned coils do not have the same number of windings on this instrument. Consequently, the precision of the DACs is more limited in one axis, leading to a slight broadening of the ring indicated by the grey arrows.

to take exposures. The conditions in the microscope are dynamic (specimen drift, lens instability) making it important to take exposures quickly before alignment conditions require readjustment. Along with diffraction pattern exposures, it is useful to record the precession amplitudes in the form of voltages and record an image of the BT circle (DS disabled) to document the cone semi-angle.

APPENDIX F

Intensity Measurement

Several methods for accurate intensity measurement are available for quantifying intensities gathered during the experiment. Serial detection using a Faraday cup sensitive single electrons has been discussed in section 2.2 (Bagdik'ianc and Alexeev 1959; Avilov et al. 1999). Parallel detection methods include film, image plates (Zukhlistov et al. 2004), and charge-coupled devices (CCDs). In this appendix, quantification of the data recorded using the parallel detection methods listed will be discussed in more detail.

The data on the recording medium is transferred into grey levels in the digital domain by means of an optical scanner. Patterns from the Al_mFe studies were measured by digitizing the negative on a light box using a CCD, obtaining 512×512 pixel images of each pattern with 8-bit precision (Berg et al. 1998). In the acquisition of intensities from $\text{La}_4\text{Cu}_3\text{MoO}_{12}$, the negatives were scanned using an Optronics P-1000 microdensitometer at $25 \mu\text{m}$ per pixel, resulting in 8-bit images approximately 2000×3000 pixels in size (Own et al. 2004).

The most basic quantification method is background subtraction followed by intensity integration, as shown in figure F.1. The background is typically approximated by a linear interpolation between points tangent to the peak tails. Often the curve can be interpolated by a polynomial spline, making analytical quantification possible. The drawback to this method is that the background is often curved,

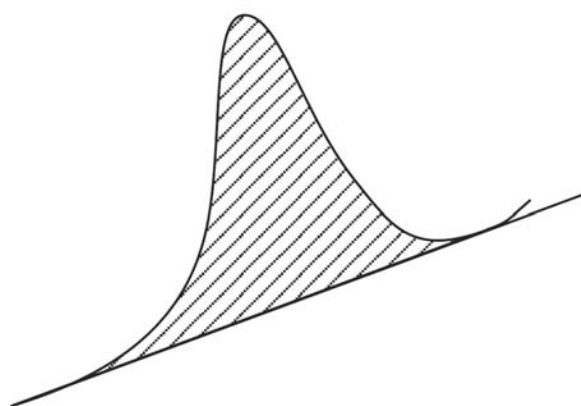


Figure F.1. Demonstration of the background subtraction technique for measuring peak intensity. The background is approximated by a line connecting points tangent to the probe tails. The background is subtracted and the area under the curve (shaded region) is integrated, or calculated from a spline approximation.

or neighboring peaks may overlap with the peak being quantified causing an overestimation of the background level.

In the the Al_mFe study, line profiles through each spot were made after background removal. Line profiling assumes each reflection exhibits perfectly circular symmetry, which is acceptable for the convergent beam case since spatial resolution constraints are more relaxed; however, with (near-) parallel illumination, the constraints are much tighter because peaks are sharper. Convergent mode precession limits measurable patterns to sparse diffraction patterns, making surfaces and superstructures more difficult to study.

Background subtraction followed by integration in two dimensions is necessary when precession patterns are not well-aligned. Patterns from the UHV H-9000 instrument demonstrated this problem often, where peak shapes were irregular and did not follow a common motif. Figure F.2(a) shows a typical diffraction spot from this system. Multiple peaks appear during different points along the precession cycle where strong excitation occurred. The optical system was not able to bring the intensity to a single point for easy measurement, so a manual routine was implemented in Synoptics Semper VI software to first identify and subtract a background level (linear), then apply a mask around the spot, and finally integrate the levels within the masked region. This method was very time-consuming but proved fairly accurate and the datasets demonstrated excellent statistics when the intensities were merged from multiple datasets (Own et al. 2004).

A resolution of 8-10 bits (2-3 orders of magnitude) — the resolution of the measurements described above — is very limited; what is desired is a large dynamic range spanning at least 3-4 orders of magnitude. The dynamic range as well as the statistical strength of the data can be improved by taking multiple measurements. In this scheme, several negatives are taken with differing exposure times in order to faithfully measure very strong beams without saturation and give weak beams a chance to be detected with suitable resolution. Negatives are individually quantified, forming separate datasets. The saturated peaks and peaks below a noise threshold within each set are discarded. The remaining peaks that are common to multiple datasets are used to scale the negatives for merging, with the intent to decrease the overall error of the merge. The scaling results in effective peaks, many of which span several measurements. A measure of their statistical error is intrinsically available and the dynamic range can readily be expanded to 4 or 5 orders of magnitude by this method.

A more sophisticated method of quantification utilizes cross-correlation, which is very accurate because of subpixel interpolation (oversampling) (Xu et al. 1994). This scheme is robust against streaking and diffuse scattering and can extract intensity from very weak spots. Additionally, it can be completely automated. In this process, a lattice is initially defined, which identifies lattice vectors \mathbf{u} and \mathbf{v} that describe spot positions to reasonable accuracy. A peak-finding algorithm samples several reflections — ideally of strong intensity with low background — and averages these after scaling to generate a cross-correlation kernel (unitary spot motif) that has a profile that models the majority of the diffraction spots in the data set. The cross-correlation algorithm then traverses all integer multiples of \mathbf{u} and \mathbf{v} , masking off a region and using the spot motif to quantify the spot intensity in a consistent fashion.

The cross-correlation method works best in conventional diffraction patterns where the spot profile is representative of the image of the electron probe — itself an image of the source — convolved with

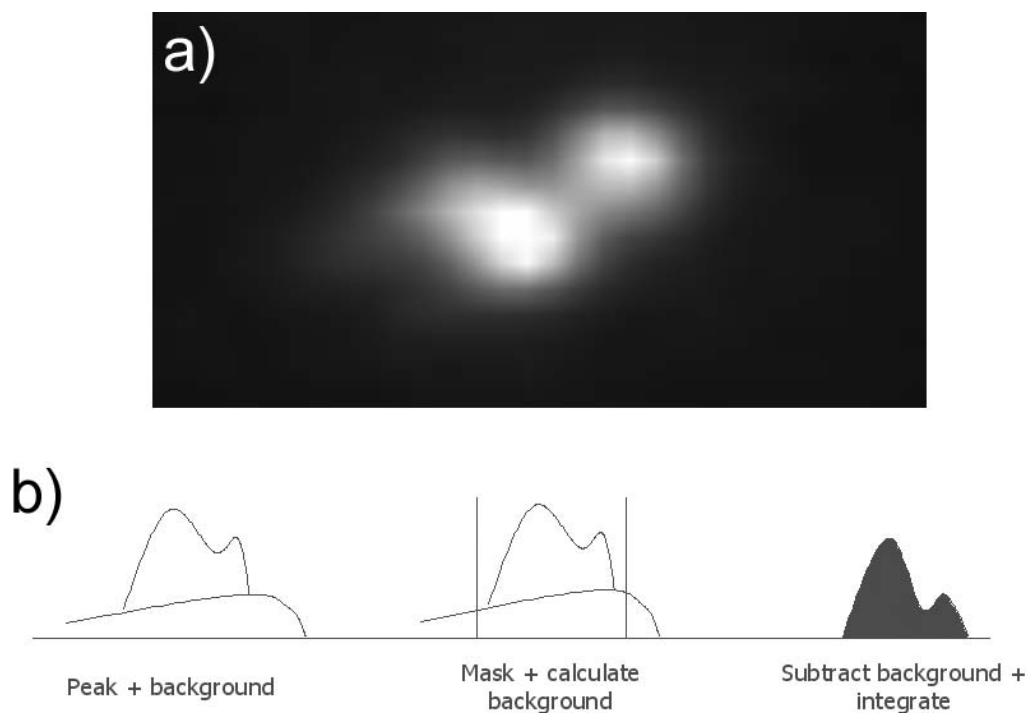


Figure F.2. Measurement of an irregular peak shape. An irregular precession spot is shown in (a). The quantification procedure is demonstrated in (b): the spot is masked, the background is subtracted, and the remaining intensity integrated.

the specimen. This is the case in selected-area and conventional electron diffraction. In precession, the peak shapes may vary because of optical aberrations and the measurement algorithm will fail if the profiles vary anisotropically in different parts of the diffraction pattern because an accurate common motif cannot be found. However, it will be successful if a common peak shape can be generated in some way. This can be accomplished by converging the illumination slightly, or ensuring very good alignment.

A cross-correlation method has been implemented by the Marks research group in the Semper software and has been reliably used to quantify many surface diffraction data sets over the past decade. The patterns taken on the newer instrument have been measured using the new EDM software (Kilaas et al. 2005), which integrates image processing, intensity measurement, and direct methods into a single software package. A comparison between the two implementations was made in order to benchmark EDM's cross-correlation implementation. An 8-bit test image was created in Semper using randomly-placed Gaussian-shaped peaks with intensities spanning over 10 orders of magnitude. A Gaussian background centered over the transmitted beam was added to simulate the decrease in scattering strength with angle. The pattern was measured by both Semper and EDM; the results are shown in figure F.3. In comparison, Semper was slightly more sensitive, being able to extract almost three orders of magnitude

from the 8-bit image whereas EDM reliably extracted intensities over 2.5 orders of magnitude. EDM's measurements coincided with the Semper results almost exactly over the measured range.

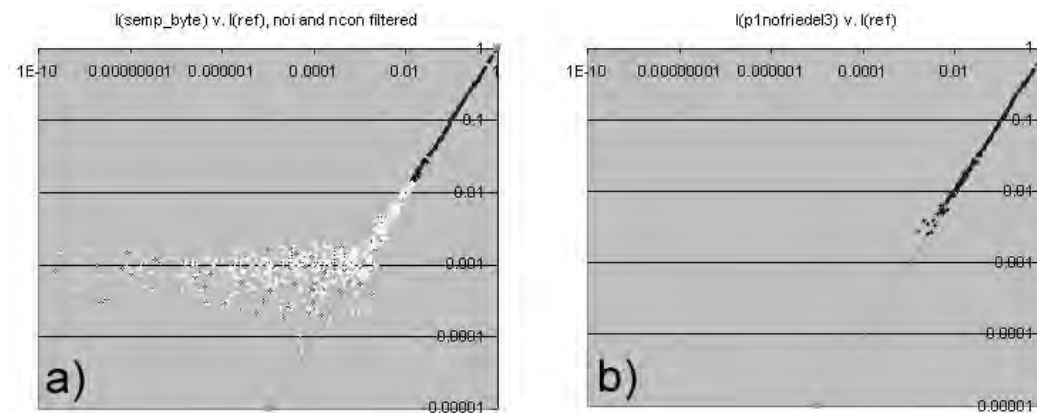


Figure F.3. (a) Semper-measured Gaussian intensity profiles. The straight line corresponds to the true spot intensities. Lighter data points correspond to low-intensity spots and spots below the noise floor (the flattened region). (b) EDM-measured intensity profiles. The cutoff is just above the noise floor measured by Semper, with very good correspondence to the true intensity over 2.5 orders of magnitude.

APPENDIX G

(Ga,In)₂SnO₄ Dataset

Table G.1: Kinematical amplitudes and experimental amplitudes for the GITO precession experiment (normalized to strongest reflection). See figure 3.2 for experimental errors. Reflections excluded in direct methods are starred (*).

h	k	g	F_{kin}	F_{prec}
1	1	0.1162	1.47E-01	6.13E-01*
-1	1	0.136	1.38E-01	5.21E-01*
2	0	0.1711	2.25E-01	5.46E-01*
2	1	0.1816	3.98E-03	2.75E-01*
0	2	0.1864	8.14E-02	3.41E-01*
1	2	0.1925	1.49E-01	4.50E-01*
-2	1	0.2072	4.52E-01	7.09E-01*
-1	2	0.2169	1.94E-01	6.43E-01*
2	2	0.2325	6.26E-02	4.15E-01*
3	0	0.2566	1.99E-01	3.54E-01
3	1	0.259	1.69E-01	5.04E-01
-2	2	0.272	4.92E-03	2.69E-01
1	3	0.2793	2.16E-01	3.19E-01
0	3	0.2796	8.81E-01	7.65E-01
-3	1	0.2864	1.80E-01	3.03E-01
3	2	0.2926	4.21E-04	2.95E-01
2	3	0.3041	6.88E-01	6.61E-01
-1	3	0.3049	1.64E-01	3.51E-01
-3	2	0.34	1.04E-01	3.84E-01
4	1	0.3403	7.82E-02	2.82E-01
4	0	0.3422	4.63E-02	2.54E-01
3	3	0.3487	2.38E-01	3.17E-01
-2	3	0.3499	1.39E-01	3.95E-01
4	2	0.3631	2.61E-01	5.38E-01
-4	1	0.3684	1.00E+00	1.00E+00
1	4	0.3692	4.51E-03	3.29E-01
0	4	0.3728	3.59E-02	3.30E-01
2	4	0.3851	3.31E-02	2.26E-01

continued on next page...

...continued

h	k	g	F_{kin}	F_{prec}
-1	4	0.3953	9.80E-02	3.07E-01
4	3	0.4066	9.76E-02	2.70E-01
-3	3	0.408	1.69E-01	3.78E-01
-4	2	0.4145	6.71E-02	2.99E-01
3	4	0.4182	1.22E-01	3.70E-01
5	1	0.4233	1.21E-01	2.64E-01
5	0	0.4277	2.22E-01	4.67E-01
-2	4	0.4338	5.70E-01	5.83E-01
5	2	0.439	1.15E-01	2.89E-01
-5	1	0.4518	1.11E-01	2.32E-01
1	5	0.4604	7.16E-02	2.81E-01
0	5	0.466	2.62E-02	2.53E-01
2	5	0.4706	8.39E-02	2.87E-01
5	3	0.473	4.74E-02	2.61E-01
-4	3	0.4745	6.15E-02	2.36E-01
-3	4	0.4845	6.91E-02	2.52E-01
-1	5	0.4868	3.66E-01	3.36E-01
-5	2	0.4926	1.37E-02	2.71E-01
6	1	0.5071	2.49E-02	2.60E-01
6	2	0.5179	3.47E-01	4.36E-01
5	4	0.5216	1.52E-02	2.38E-01
4	5	0.5332	6.38E-02	3.06E-01
-6	1	0.5358	3.08E-02	2.39E-01
-4	4	0.544	3.66E-01	3.82E-01
-5	3	0.5464	2.58E-01	4.11E-01
2	6	0.5586	7.44E-01	5.24E-01
0	6	0.5592	1.65E-01	3.27E-01
-3	5	0.5661	6.60E-02	2.48E-01
-6	2	0.5728	4.36E-01	4.18E-01
3	6	0.5776	6.87E-02	2.31E-01
-1	6	0.5788	1.37E-02	2.39E-01
6	4	0.5853	6.19E-02	2.36E-01
7	2	0.5987	2.08E-01	2.87E-01
7	0	0.5988	5.03E-02	2.94E-01
4	6	0.6082	4.42E-02	2.73E-01
-5	4	0.6098	1.60E-01	2.42E-01
-4	5	0.6198	3.29E-02	2.59E-01
7	3	0.62	1.45E-02	2.45E-01
6	5	0.637	4.51E-01	4.14E-01
1	7	0.6446	1.39E-01	2.56E-01
5	6	0.6487	9.06E-02	2.43E-01

continued on next page...

...continued

h	k	g	F_{kin}	F_{prec}
-3	6	0.6507	3.08E-02	2.58E-01
0	7	0.6524	1.85E-01	3.54E-01
3	7	0.6626	2.44E-01	2.42E-01
8	1	0.6761	3.75E-01	3.70E-01
-6	4	0.6799	5.63E-02	2.39E-01
7	5	0.6989	1.04E-01	2.38E-01
-7	3	0.6994	3.44E-02	2.69E-01
-2	7	0.6998	5.12E-01	4.44E-01
5	7	0.722	8.62E-05	2.51E-01
8	4	0.7263	3.11E-01	2.86E-01
-8	2	0.7369	5.04E-01	3.31E-01
1	8	0.737	1.99E-02	2.64E-01
-6	5	0.7453	4.77E-01	4.18E-01
7	6	0.7527	1.72E-01	2.32E-01
-7	4	0.7532	7.52E-02	3.02E-01
-5	6	0.7553	1.23E-02	2.44E-01
9	2	0.7633	7.26E-02	2.70E-01
-1	8	0.7636	3.23E-02	2.38E-01
-9	1	0.7899	1.37E-01	3.46E-01
2	9	0.8294	3.29E-01	2.90E-01
6	8	0.8364	1.66E-01	3.66E-01
10	1	0.8459	1.52E-01	2.61E-01
4	9	0.8549	2.41E-01	2.45E-01
10	0	0.8554	4.02E-03	2.76E-01
-4	8	0.8676	1.70E-01	2.33E-01
10	4	0.878	2.78E-01	2.84E-01
-8	5	0.8861	1.76E-01	2.45E-01
-9	4	0.9064	6.00E-02	3.77E-01
-3	9	0.9147	1.20E-01	2.54E-01
1	10	0.9225	1.14E-01	2.52E-01
11	1	0.931	1.67E-01	2.38E-01
0	10	0.932	3.48E-01	3.69E-01
-10	3	0.9406	3.05E-01	2.66E-01
-7	7	0.952	1.67E-01	2.94E-01
-6	8	0.969	2.84E-01	3.52E-01
-2	10	0.9735	2.50E-01	2.70E-01
10	7	0.9913	1.80E-01	2.44E-01
12	3	1.0208	1.64E-01	2.73E-01
12	0	1.0265	2.49E-01	2.91E-01
-12	1	1.0452	2.28E-02	2.31E-01
-10	6	1.0928	4.17E-01	2.63E-01

continued on next page...

...continued

h	k	g	F_{kin}	F_{prec}
13	1	1.1013	1.23E-01	2.44E-01
-12	3	1.1053	2.41E-01	2.63E-01
11	8	1.1054	4.00E-02	2.35E-01
4	12	1.1172	1.92E-01	2.74E-01
-4	11	1.1304	3.22E-01	2.60E-01
-1	12	1.1349	3.66E-02	2.56E-01
8	11	1.1401	1.74E-01	2.25E-01
-10	9	1.2883	2.42E-01	2.43E-01
-11	8	1.2887	2.80E-02	2.35E-01
-14	4	1.3088	8.89E-02	2.27E-01
-4	14	1.3997	1.15E-01	2.61E-01

table end.